International Journal of Aeronautics and Astronautics
https://dergipark.org.tr/en/pub/ijaa

2022, VOL:3, ISS:2, 71-86 e-ISSN: 2757-6574

Research Article

Aerodynamic efficiency analysis of variable morphing wings

Erdoğan Kaygan[1]*, Aslıhan Tuğce Köroğlu[2], Melisa Başak[3]

[1] *School of Aviation, Girne American University, Kyrenia, PO Box 5, 99428, Cyprus*
[2] *Aerospace Engineering Department, Middle East Technical University, Guzelyurt, 99738, Cyprus*
[3] *Aerospace Engineering Department, Middle East Technical University, Ankara, 06800, Türkiye*

Received	Revised	Accepted
March 16, 2022	April 21, 2022	July 4, 2022

Keywords
Aerodynamics
Drag
Morphing
Sweep
Twist

ABSTRACT

In this paper, variable wing and/or winglet concepts are investigated. The impetus for the work was to identify and optimize wing and winglets to enhance the aerodynamic efficiency of a morphing aircraft. The analysis is based on changing sweep angle and wing-tip twist together with cant angle morphing ($\Gamma = 0° - 45°$ $\varphi = -10° - 10°$ and $\Lambda = 0° - 30°$). A variety of cases are examined through an aerodynamic analysis tool (VLM) comparing with baseline sweep wing configuration. As a result, significant improvements in flight characteristics are observed by adapting the required angle to receive optimum performance benefits.

* Corresponding author, e-mail: ekaygan@gau.edu.tr

Nomenclature

C_D	Drag coefficient	U_∞	Freestream velocity
C_L	Lift coefficient	α	Angle of attack
C_p	Pressure coefficient	φ	Twist angle
C_m	Pitching moment coefficient	Λ	Sweep angle
L/D	Lift to drag Ratio	Γ	Dihedral or cant angle

Authorship contribution statement for Contributor Roles Taxonomy

Erdogan Kaygan, *Writing - original draft, investigation, visualization, supervision, conceptualization, methodology, software, formal analysis, writing.* **Aslıhan Tuğce Köroğlu,** *Investigation, visualization, supervision. writing – review & editing.* **Melisa Başak,** *Conceptualization, methodology, software, formal analysis, writing – review & editing.*

Conflicts of Interest: The authors declare no conflict of interest.

Citation: *Kaygan, E., Köroğlu, A.T., Başak, M. 2022. Aerodynamic efficiency analysis of variable morphing wings. International Journal of Aeronautics and Astronautics, 3, 2, 71-86.*

1. Introduction

Morphing aircraft is a flight vehicle that changes the configuration of geometry during flight to adapt itself to different flight missions. In recent years, adaptive wing and/or winglet concepts have been prominent by most aeronautical researchers very widely. Although this idea seems to be new, Wright brothers have already attempted by using twist wing concepts to create roll control of the first powered, heavier than air vehicle [1]. Due to increased demand for air transportation, this idea is no longer available.

The morphing wing concept has significant benefits such as noise reduction, improved ride quality, enhanced maneuverability, shorter landing requirements, extensive versatility, safer missions considering passengers' life and aircrafts' designs [2,3,4]. Traditional control systems (with fixed geometry and/or location) give high aerodynamic performance over a fixed range and for a limited set of flight conditions. Outside of this range, these traditional systems can be neutral or negatively influence aerodynamics and hence often give lower efficiency [2]. Since the lift requirements for aircraft will differ within a typical flight due to fuel burn, fixed- position, conventional wings with traditional control surfaces do not provide the optimal solution for aircraft performance in all flight regimes. Thus, variable morphing ideas began to look for future aircraft designs.

Over the last few decades, a number of morphing mechanisms for both fixed and rotating wing applications have been investigated, with huge potential benefits as well as drawbacks [2, 5, 6, 7] addressed, but the majority of ideas have been restricted due to issues such as excess weight, expense, structural integrity, skin configuration, and smooth surface design [8, 9, 10, 11, 12]. Neal et al. [13] studied on a variable planform aircraft that can resize its wingspan. Wind tunnel tests showed that throughout a range of lift coefficients, variable planform leads to low drag values. Blondeau et al. [14] accomplished to 114% change in the aspect ratio of a wing for an unmanned aerial vehicle (UAV). Although they experimentally achieved to increase lift to drag ratio by 25% when the wingspan is fully extended, the mechanism was reported due to fabrication problems. Similarly, Joo et al. [15] investigated a scissor wing-box mechanism with the help of a distributed network of actuators. Springs were used to adjust the skin by stretching, but a parametric study of the compliance was not fulfilled. Moreover, variable sweep wing design has been the most successful and popular morphing design so far. By sweeping the wing, an aircraft can fly at both supersonic and subsonic speeds. It also helps the aircraft in take-off and landing which are the most crucial stages of flight. Pivoting of the wing implemented in many successful and operating aircrafts such as Bell-X-5, F-111, F-14, and B-1. Although these variable-sweep wing designs are successfully accomplished, they encountered many challenges, too. One of the major challenges faced by the designer of X-5 was to compensate for the change in the center of gravity location of the airplane as the wing is rotated about its pivot [16]. Though F-111 went into the production line for the Air Force, it encountered several problems due to structural failures, loss of directional stability, engine surge, and stall but these problems were solved by a major inlet redesign [5]. Also, sweep variation has been done by using bi-stable composite spars and smart materials [17]. Due to various numbers of successful attempts in variable-sweep wing design, the concept is investigated for its further implementation on the newly designed morphing wing.

The oldest form of morphing is varying the twist distribution of the wing to improve flight performance and control authority of the air vehicle. Changing the twist in the outboard parts of the wings will increase the required control forces needed for maneuvering flight, according to a review of early designs and approximation techniques [2]. Winglet and/or wingtip twist may improve performance in a similar way to wing twist concepts [18]. The adaptive wing-tip concept is based on a chiral internal structure that allows for controlled cant angle orientation, camber, and twist across the entire flight envelope [19]. Similar to wing morphing concepts, previous surveys and investigations have shown that winglets and/or wingtip devices can reduce induced drag while also improving an aircraft's range and aerodynamic efficiency. In addition, several studies have discovered that winglets can reduce CO_2 emissions by up to 6% and NOx emissions by up to 8%. NASA tested a variety of drag-reducing and wingtip

https://doi.org/10.55212/ijaa.1088399

products, finding that winglets can increase aircraft efficiency by 10-15% during the cruise. Later, most commercial long-range aircraft were equipped with winglets to reduce induced drag and save fuel [20].
Furthermore, several studies looked at a new approach to controlling aircraft using adaptable winglet principles. The adjustable cant angled winglets were investigated by Bourdin et al. [21] Kaygan et al. [22] – [24]and Gatto et al. [25] to improve the aerodynamic efficiency and control of flying wing aerial vehicles. Woods et al. [26] first proposed the fish-bone active camber wing design. The Fish-Bone Active Camber (FishBAC) design is based on a flexible skeletal system influenced by fish anatomy. Wind tunnel research revealed that using the FishBAC morphing structure, a significant improvement in the lift-to-drag ratio of 20%–25% was achieved across the range of angles of attack as compared to the flapped airfoil.
In this paper variable morphing concepts investigated numerically to illustrate the aerodynamic performance benefits of an aerial vehicle. The investigation of the principal variables is involved by changing the wing sweep, cant, and winglet twist angle. Hence, the remaining sections of this paper will describe the computational methodologies and aerodynamic analysis of selected cases.

2. Methodology

2.1 Airfoil selection

Since the airfoil is one of the most important parts which determines the performance of the wing, selection of the airfoil is a crucial stage in the design process. JavaFoil and XFOIL software are utilized in the airfoil selection process. JavaFoil is a straightforward program that employs standard analysis methods such as potential flow analysis with a higher-order panel approach and boundary layer analysis using the integral technique [27]. The panel method is based on taking a list of airfoil coordinates and defining the local and inviscid flow velocity along a surface at any chosen angle of attack using a linearly increasing velocity distribution. The integral technique, on the other hand, seeks to solve differential equations by starting at the stagnation point and proceeding around the top and lower surfaces of the airfoil. Since JavaFoil does not mimic laminar separation bubbles or turbulent flow separation, the findings will be inaccurate in the presence of greater regions of flow separation [27].

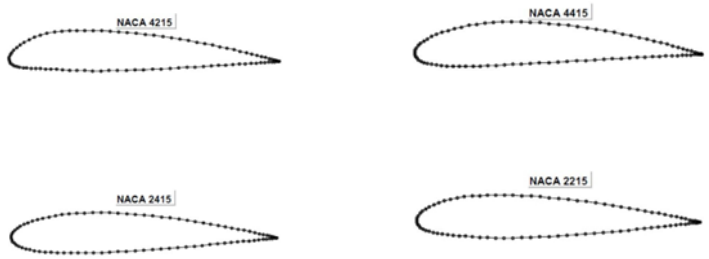

Fig. 1. NACA 4-series airfoils

Table 1. Airfoil comparison

Airfoils	C_{Lmax}	C_{m0}
NACA2415	1.40	-0.032
NACA4415	1.72	-0.096
NACA4215	1.74	-0.059
NACA2215	1.62	-0.032

https://doi.org/10.55212/ijaa.1088399

Furthermore, the XFOIL program is conducted to analyze the flight characteristics at high angles of attack in detail. XFOIL is a graphical user interface for building and evaluating isolated subsonic airfoils. It is composed of a succession of menu-driven routines that carry out a range of critical functions. It can solve viscous and inviscid flows over an airfoil for subsonic flows. Unlike JavaFoil, XFOIL is capable of predicting transitional separation bubbles [28]. Angles of attacks beyond C_{Lmax} are also assessed by taking its benefits into account.

Figure 1 illustrates the shape of NACA 4-series Airfoils. Among the analyzed airfoils, NACA4415 is selected to satisfy good compromise between high C_{Lmax} and low C*m*0 (seen in Table 1 and Figure 2). Even NACA4215 has a slightly higher C_{Lmax} value, NACA4415 has a much lower Cm0 value than NACA4215 which is as important as C_{Lmax} since having low C*m*0 improves stability characteristics. Also, it can be seen from Figure 2, the slope of C_L/C_D graph of NACA4415 is higher compared to others which helps to maintain a high lift to drag ratio during flight. Since L/D ratio is directly related to efficiency, keeping this value as high as possible provides optimum flight conditions.

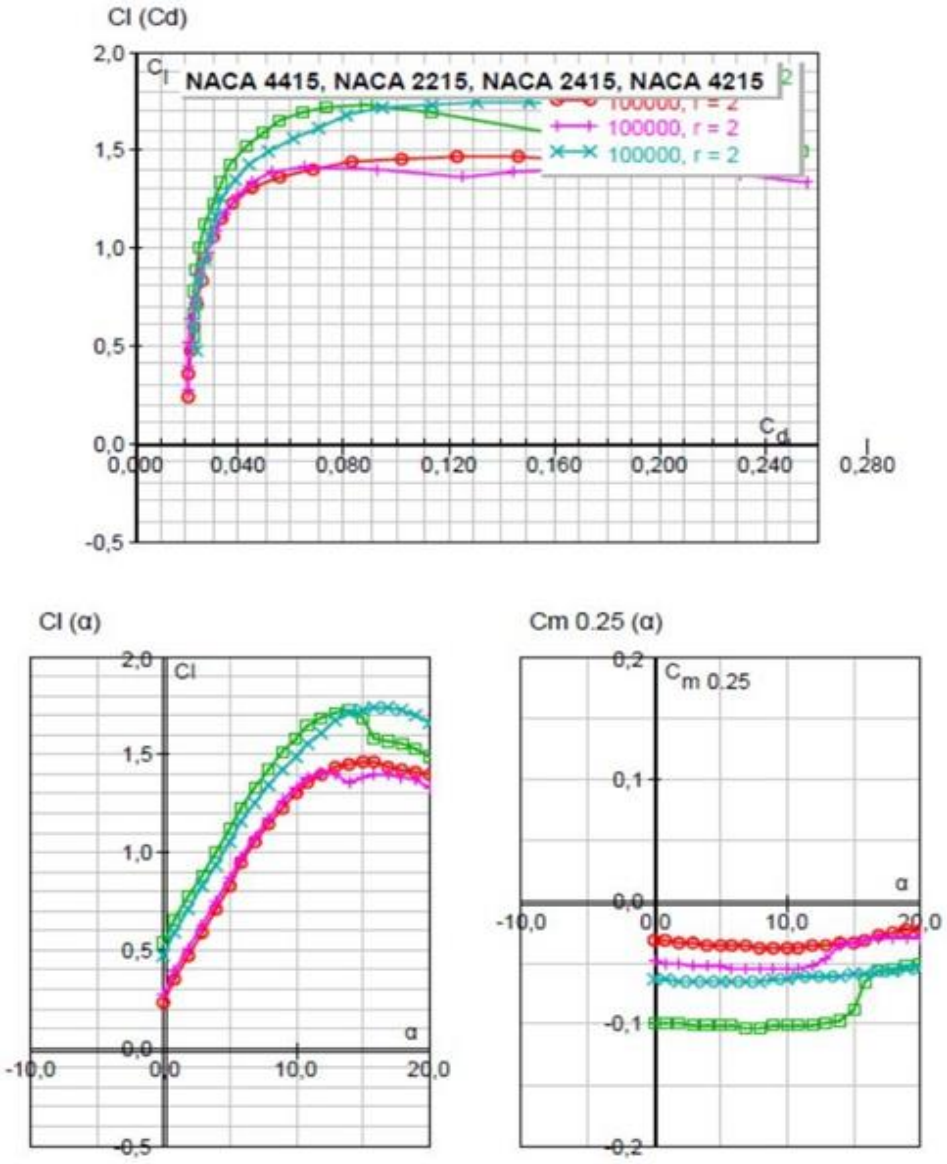

Fig. 2. Airfoil polars obtained by JavaFoil

https://doi.org/10.55212/ijaa.1088399

Table 2. Parameters for aerodynamic analysis

Polar Type	Fixed Speed (10 m/s) - Inviscid
Reynolds Number	100.000,00
Mesh Elements	546
Density	1.2041 kg/m^3
Kinematic Viscosity	1.5065 x 10−5m^2/s

2.2 Aerodynamic modelling and computational methods

Numerical analysis of the morphing wing is carried out using XFLR5 software. XFLR5 is a tool to analyze airfoils, wings, and planes operating at low Reynolds Numbers. For straight wings with a moderate to the high aspect ratio, Prandtl's Lifting Line Theory produces satisfactory results. Classical Lifting Line Theory, on the other hand, is ineffective for low- Aspect Ratio straight wings, swept wings, and delta wings. For this reason, Vortex Lattice Method is used to compute the variations of aerodynamic coefficients [29, 30].

In this method, the wing is covered by a finite number of panels. A series of horseshoe vortices are superimposed such that every panel has a horseshoe vortex represented by a group of letters. This lattice of horseshoe vortices covers the whole wing, each with a distinct vortex strength. The Biot-Savart Law is used to calculate the normal velocity caused by all horseshoe vortices at any control point. When the flow-tangency condition is applied to all control points, a system of simultaneous algebraic equations emerges, which may be solved to determine the unknown vortex strengths. Table 2 shows the simulation properties of morphing wings. According to grid refinement analysis specific mesh size was used. In addition to mesh size, Reynolds number and density used because of the atmospheric conditions. Also, Figure 3 and Figure 4 illustrate the aerodynamic modeling of morphing wing.

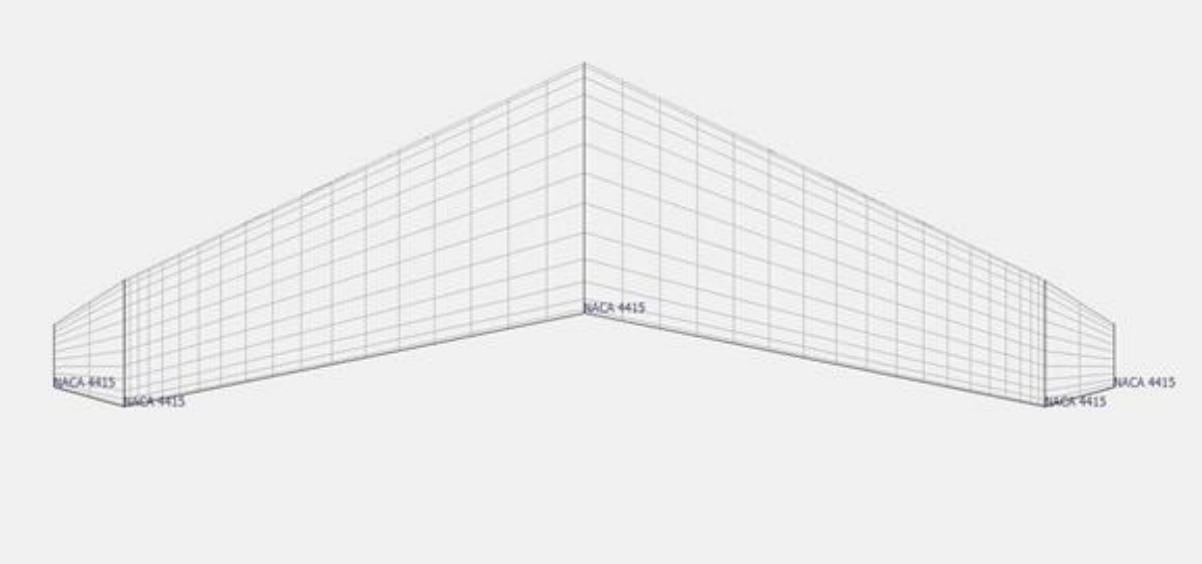

Fig. 3. Aerodynamic model of morphing wing

https://doi.org/10.55212/ijaa.1088399

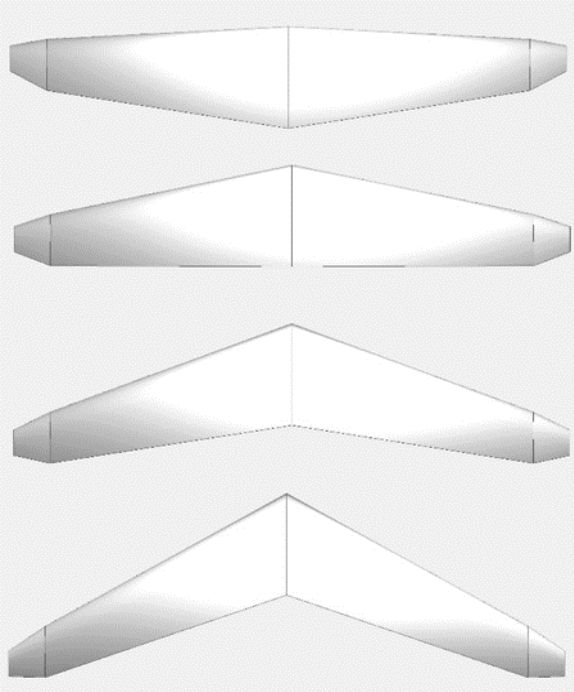

Fig. 4. Morphing Sweep Wing (From 0° to 30°)

3. Results and Discussion

3.1. Variable sweep angle

Figure 5 represents the variations of C_L, C_D, C_L/C_D, and C_m with respect to morphing sweep angles. The sweep angle varies between 0° to 30°. It can be seen from the C_L graph that the highest value of the lift coefficient occurs at $\Lambda = 10°$, regardless of the angle of attack. The lowest value of C_L occurs at $\Lambda = 30◦$, and the lines of $\Lambda = 0$ and $\Lambda = 5◦$ are top of each other. As the sweep angle increases, the value of C_L decreases, except for the sweep angle of 10. This is an expected result since increasing the wing sweep decreases the lift coefficient as agreements with [18].

According to C_D curves, $\Lambda = 10◦$ has the highest drag values, except for the very low α ranges. Regardless of the α, $\Lambda = 30°$ has the lowest C_D value. At the low α, $\Lambda = 0°$ curve has the highest C_D values, while, at the high α, $\Lambda = 10°$ induces more drag overall sweep angle morphing scenarios. These results are also proved that why most of the commercial airplane has the 30°- 40° of sweep wing configuration (to reduce fuel consumption by decreasing drag force) [31].

As the wing morphs from 0° to 30°, a significant increase in C_L/C_D has also been observed. At the low α values, $\Lambda = 0°$ has the lowest L/D ratios. Besides, at the high α, $\Lambda = 10°$ has the lowest aerodynamic efficiency. Regardless of α, $\Lambda = 30°$ has the best aerodynamic efficiency. Observing the highest L/D at $\Lambda = 30°$ is an expected result because sweeping the wing further decreases the C_L. As C_L decreases, C_D curve decays more, accordingly, C_L/C_D values are increased while morphing from 0° to 30°. While changing the Λ from low to high angles, the pitching moment coefficient decreases linearly with increasing α. As a result, it is possible to provide optimum flight performance by having higher L/D ratios with $\Lambda = 30°$, this situation enhances the stability characteristics at high angle of attacks. Figure 5 illustrates the morphing sweep in a wing with angles varying between $\Lambda = 0°$ to $\Lambda = 30°$.

https://doi.org/10.55212/ijaa.1088399

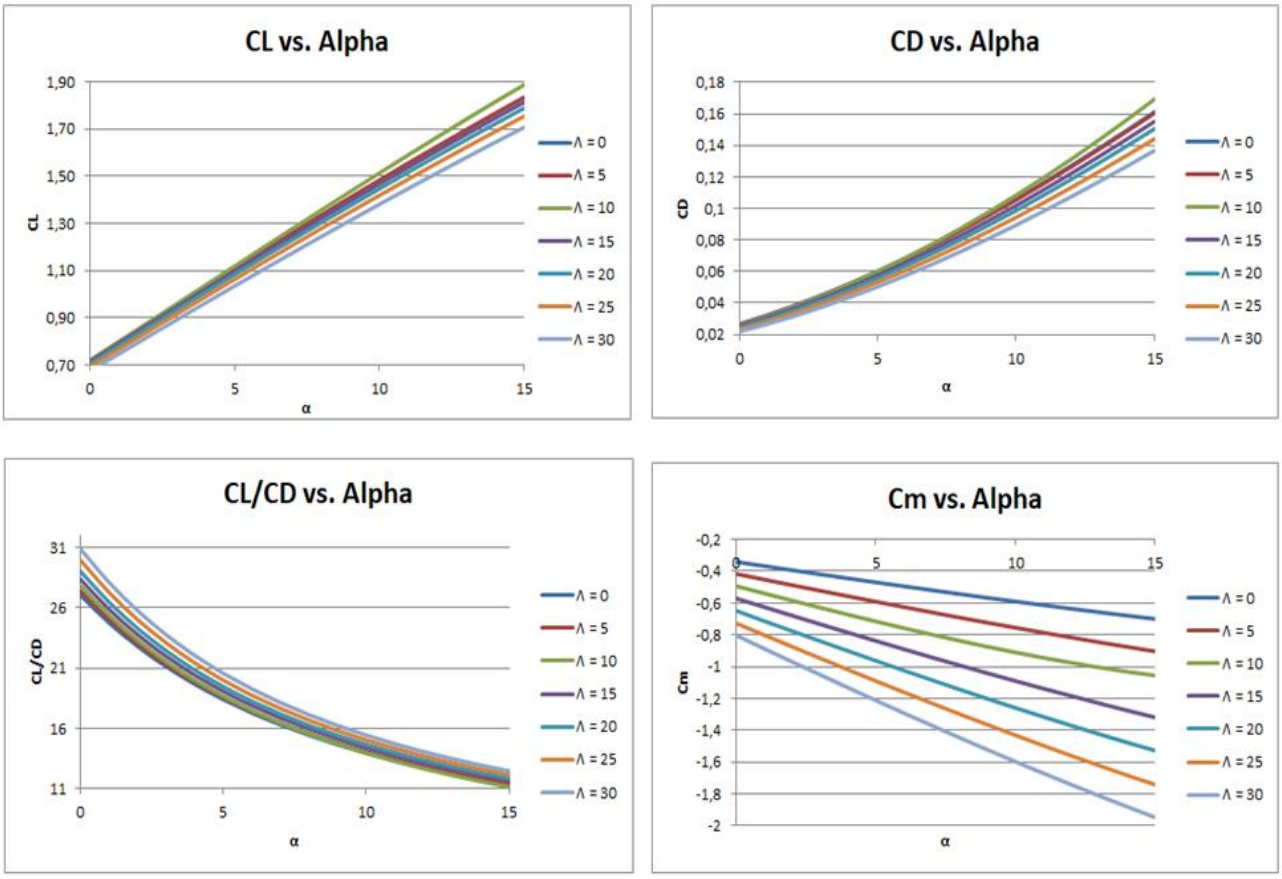

Fig. 5. Effect of morphing sweep angle

Table 3. Increase in efficiency [%]

Sweep Angle [°]	α = 0	α = 5°	α = 10°	α = 15°
5	1.28	0.87	0.68	0.58
10	2.88	1.37	-0.06	-1.94
15	4.87	3.65	3.09	2.76
20	7.34	5.71	4.95	4.50
25	10.76	8.66	7.66	7.06
30	14.22	11.73	10.51	9.77

Table 3 also represents the increase in efficiency percent with respect to the angle of attack, considering different Λ values. Positive values indicate the increase in efficiency. The increase in efficiency percentages is calculated using the baseline wing as a reference. The highest efficiencies were achieved at α = 0. It can be seen from the table that after α = 10°, Λ = 10° becomes inefficient. As α increases, the largest decrease occurs at Λ = 10°. At Λ = 5°, the increase in efficiency is slightly decreased, as the angle of attack increases. As a result, the most efficient sweep angle was found to be Λ = 30°, regardless of the angle of attack. This is a predictable result since a significant increase was observed for this sweep angle in C_L/C_D graph as agreement with [32, 33, 34]

https://doi.org/10.55212/ijaa.1088399

3.2 Winglet twist morphing

Figure 6 represents the variations of C_D, C_L, C_L/C_D, and C*m* with respect to morphing winglet twist angles. During computations, cant angle and sweep angle considered as $\Gamma = 45°$ and $\Lambda = 20°$, respectively. It can be seen from the C_L graph; the highest value of C_L occurs at $\varphi = 10°$ and the lowest value of C_L occurs at $\varphi = -10°$ at all α values. This would be expected due to increased effective angle of attack at positive twist angle tends to raise lift coefficient further [20, 23, 35]. Comparing with C_D graph, the differences of the C_L values change dramatically with increasing angle of attack. This leads to an improved L/D ratio at $\varphi = -10°$ at a higher angle of attacks. Yet, at low angle of attacks, morphing to $\varphi = -5°$ results in higher C_L/C_D.

According to the C_D graph, the highest value of C_D occurs at $\varphi = 10°$ and the lowest value of C_D occurs at $\varphi = -10°$ at high α values. However, at low α values, the curves were observed to be very close to each other. Considering C_L/C_D graph, at low angle of attacks, the curves of $\varphi = -5°$ and $\varphi = 5°$ overlap and have the highest C_L/C_D value. By increasing the angle of attack, the curves start to separate and overlap again with a different combination. The highest C_L/C_D values observed to be at $\varphi = -10°$ and $\varphi = -5°$, as the angle of attack increases. The lowest C_L/C_D value observed to be at $\varphi = 10$ due to high drag values in all ranges of α. However, the C_L/C_D values are very compatible with each other.

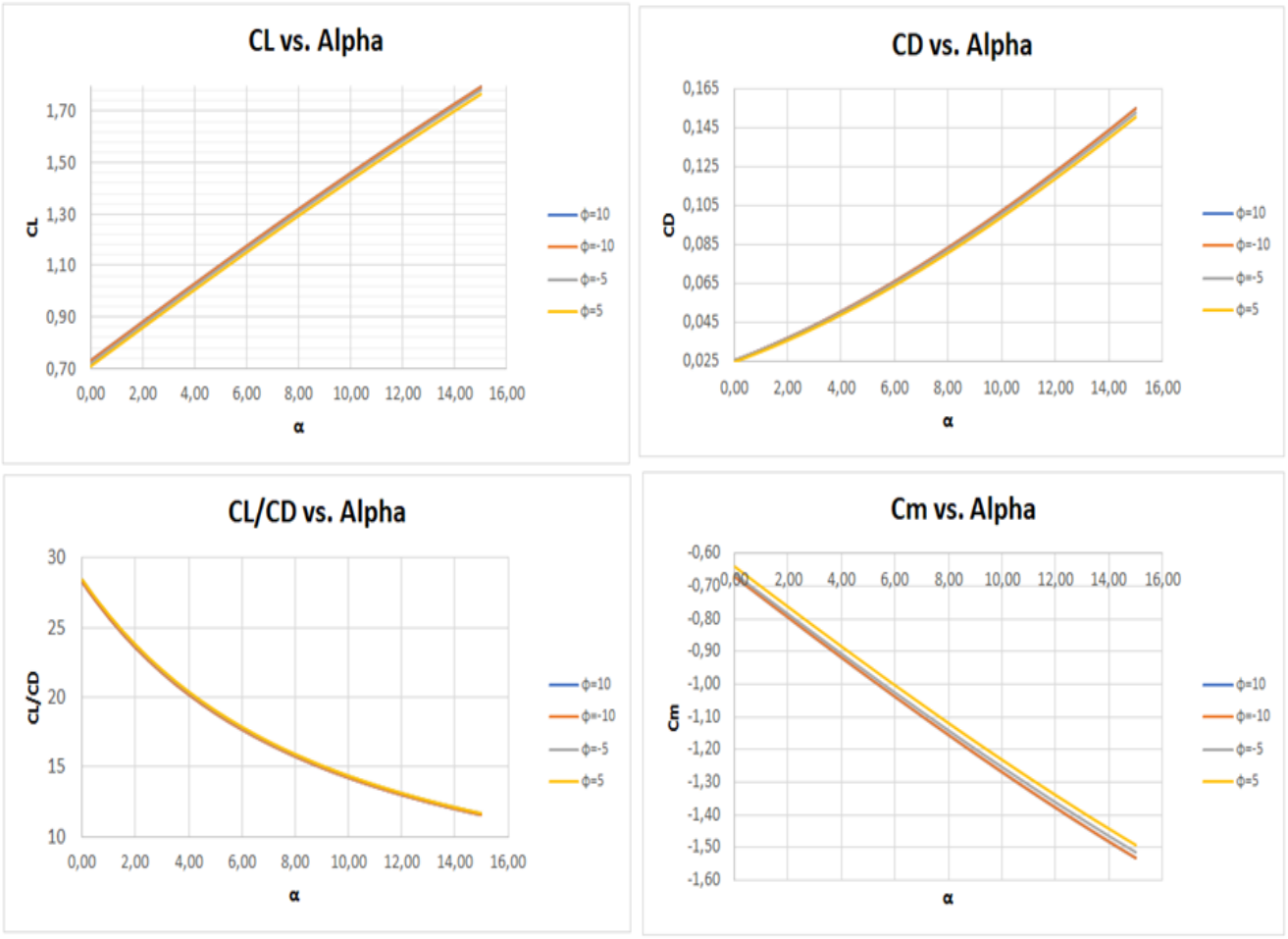

Fig. 6. Effect of winglet twist angle

https://doi.org/10.55212/ijaa.1088399

Table 4, Table 5, and Table 6 represent the drag reduction percent for different φ values. To compare positive twist values, negative twist cases indicate drag reductions. The sweep angle kept constant as Λ = 20°. The drag reduction percentages are calculated using the baseline wing as a reference. The cant angle values are chosen as Γ = 45° and Γ = 80° according to [36]. 80° is recommended for flight phases such as ground operations and landing, 45° is recommended for flight phases such as take-off, initial climb, cruise, and descent.

Table 4. Drag reduction at Γ = 0°

	α = 0		α = 15°	
Twist Angle [\degree]	C_D	**Drag Reduction [%]**	C_D	**Drag Reduction [%]**
-10	0.024227	0.31	0.148525	1.36
-5	0.024180	0.50	0.149488	0.72
5	0.024573	-1.12	0.151934	-0.90
10	0.025023	-2.97	0.153659	-2.05

Table 5. Drag reduction at Γ = 45°

	α = 0		α = 15°	
Twist Angle [\degree]	C_D	**Drag Reduction [%]**	C_D	**Drag Reduction [%]**
-10	0.024827	0.68	0.149928	1.23
-5	0.024824	0.70	0.15079	0.66
5	0.025331	-1.33	0.153044	-0.82
10	0.025857	-3.44	0.15464	-1.87

Table 6. Drag reduction at Γ = 80°

	α = 0		α = 15°	
Twist Angle [\degree]	C_D	**Drag Reduction [%]**	C_D	**Drag Reduction [%]**
-10	0.026131	1.38	0.155810	0.72
-5	0.026218	1.05	0.156297	0.41
5	0.026949	-1.7	0.157773	-0.53
10	0.027616	-4.23	0.158876	-1.23

According to the drag reduction results given in Table 4, Table 5, and Table 6, -10 degrees of twist angle with 80 degrees of cant angle observed to be the most efficient in terms of drag reduction at α = 0°. However, at high angle of attack values, the drag coefficient is found to be highest at φ = 10°, as mentioned. Thus, as the angle of attack increases, the drag reduction values are changed accordingly. Finally, at a low angle of attack, the most efficient twist angle was found to be φ = -10° with Γ = 80◦ and Λ = 20°. Besides, the wing with the same twist and sweep angle has the highest drag reduction at a high angle of attack. As a result, cant angle morphing at various flight regimes reduces drag and gives optimum flight capabilities as agreement with [32, 34].

Figure 7 represents the C_L and C_D variations along with different cant angles for each φ = −10°, −5°, 5°, and 10°. To see the effect of twist clearly, besides Γ = 45◦, a range of cant angles are observed within this analysis. As can be seen, C_D curves overlap for a wide range of cant angles, while C_L curves have major differences.

https://doi.org/10.55212/ijaa.1088399

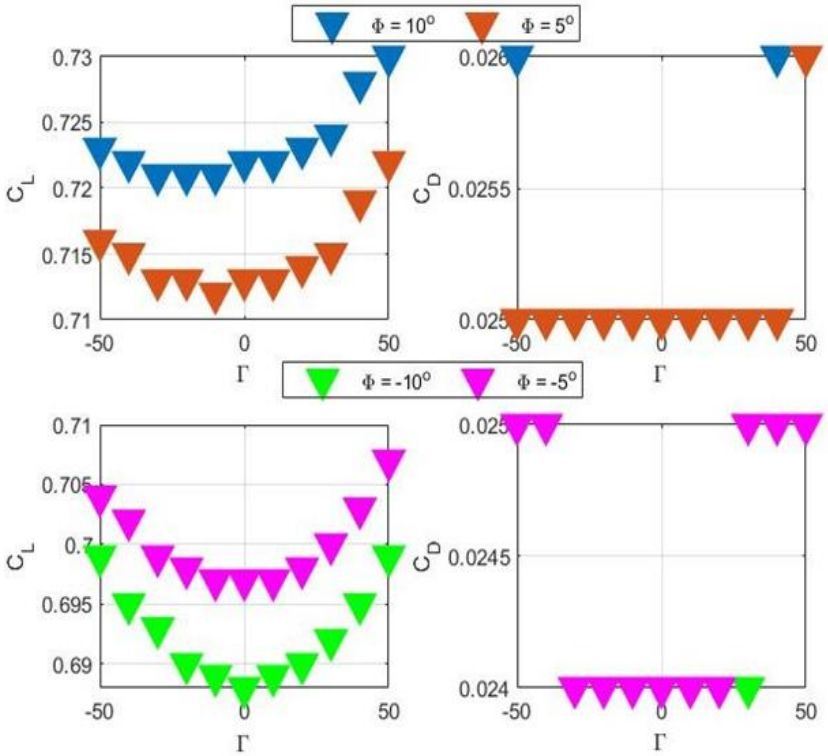

Fig. 7. Cant angle variation versus CL and CD at α = 4° and Λ = 20°

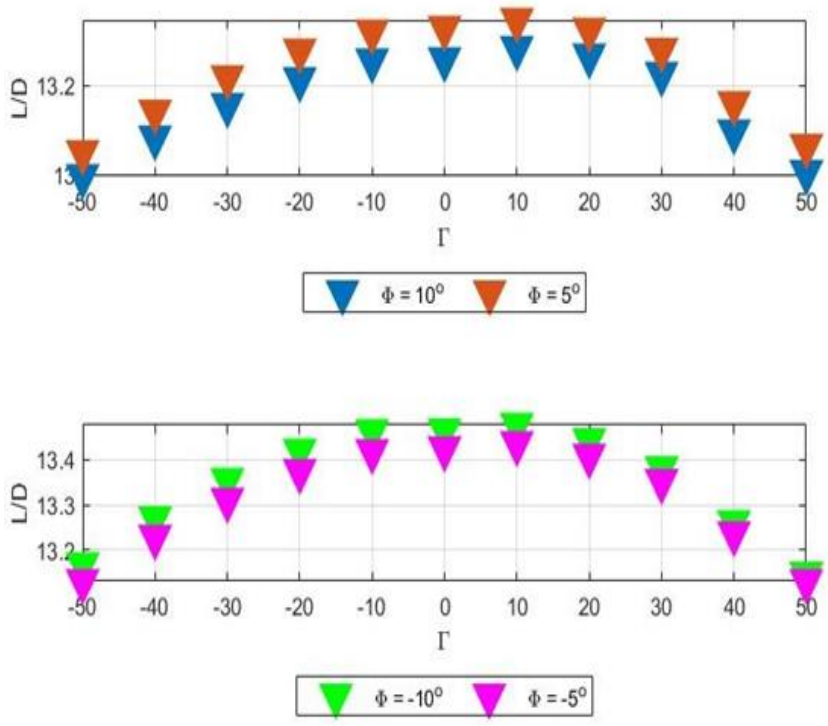

Fig. 8. Cant angle variation versus L/D at α = 4° and Λ = 20°

Figure 8 represents the C_L/C_D variations over a range of specified cant angles. For negative twist values, Γ = −5° and Γ = −10° have the highest aerodynamic efficiency, although there is a slight difference. However, for positive

https://doi.org/10.55212/ijaa.1088399

and all twist values, Γ = 0° has the highest aerodynamic efficiency. This would be expected due to increased and or decreased dihedral value that creates an overall reduction in C_L and C_D as agreement with previous works [18, 37, 38].

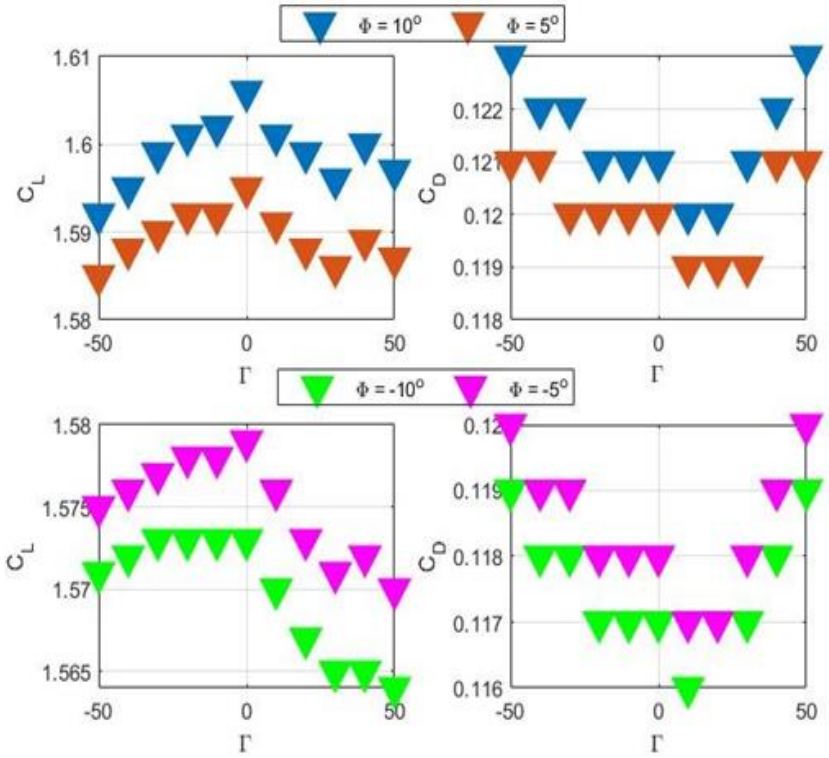

Fig. 9. Cant Angle Variation versus CL and CD at α = 12° and Λ = 20°

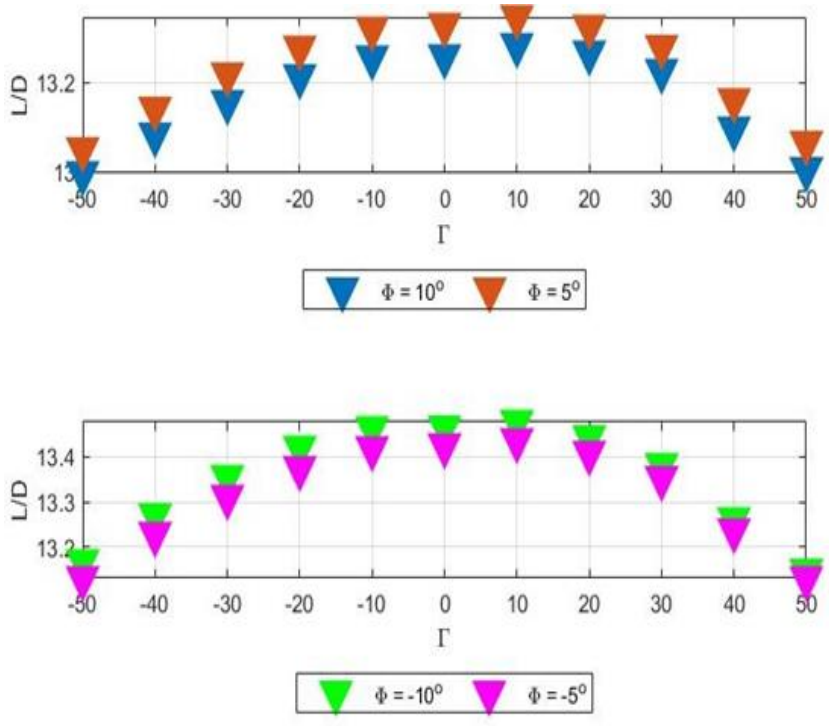

Fig. 10. Cant Angle Variation versus L/D at α = 12° and Λ = 20°

https://doi.org/10.55212/ijaa.1088399

In Figure 9 and Figure 10, the angle of attack has been increased from 4° to 12° for the same twist and cant angle values. As can be seen, C_D curves significantly changed, and C_L curves with negative twist values started to have a different manner from the previous results. At C_D curves, higher cant angles being both positive and negative resulted in higher drag forces. Due to the increase in the angle of attack thereby drag force, L/D values decreased, as expected. Being all twist values resulted in almost the same values, the most efficient cant angle is decided as 10° for $\alpha = 12°$ and $\Lambda = 20°$.

Figure 11 represents the C_L and C_D variations over the same cant angle range at $\alpha = 4°$ and $\Lambda = 30°$. By morphing sweep angle from $\Lambda = 20°$ to $\Lambda = 30°$, higher C_L values were observed with the doubled drag coefficient values for all cases of twist angle. For negative values of twist, C_L curves have the same decreasing and increasing manner, but the local minimum of these curves is $\Gamma = 10°$, it was $\Gamma = 0°$ at $\Lambda = 20°$. For positive cases of twist, C_L curve of $\varphi = 5°$ preserves its values over a wide range of cant angles, and found as the most efficient twist angle for $\alpha = 4°$ and $\Lambda = 30°$. Besides, by increasing sweep to $\Lambda = 30°$, $\varphi = 10°$ as the most efficient one at the $\Lambda = 20°$ case- replaced with $\varphi = 5°$.

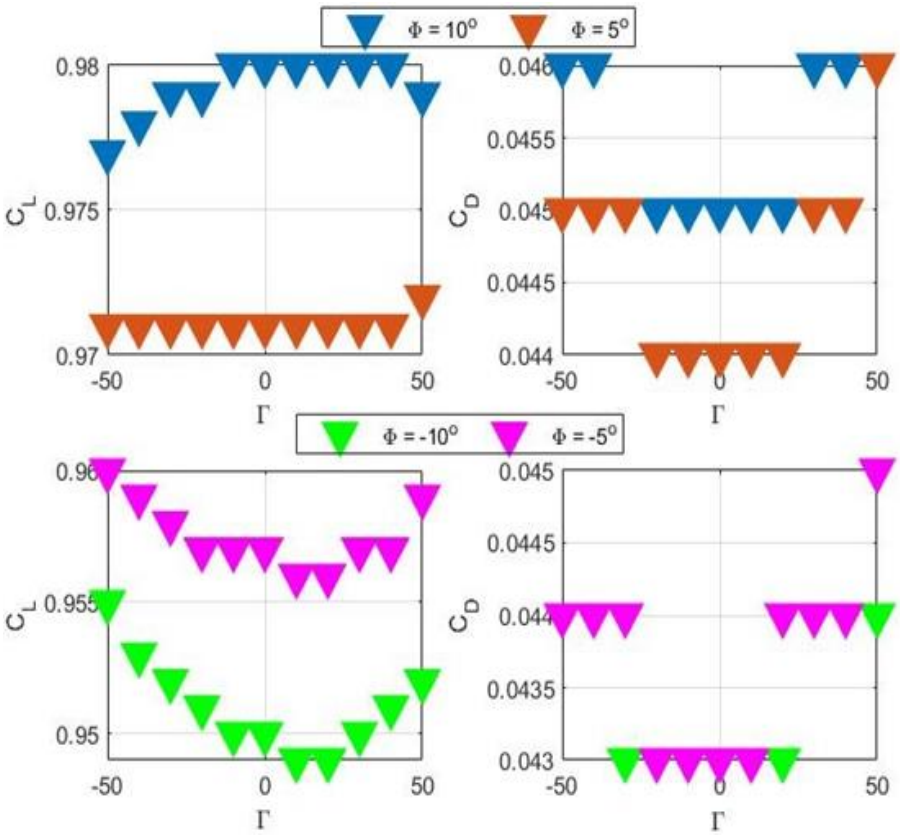

Fig. 11. Cant angle variation versus C_L and C_D at $\alpha = 4°$ and $\Lambda = 30°$

To compare L/D curves, Figure 12 shows the variation of analyzed twist values over the specified range of cant angles at $\alpha = 4°$ and $\Lambda = 30°$. As can be seen, curves that include negative twist values overlap. For positive twist angles, $\varphi = 5°$ achieved slightly better efficiency over $\varphi = 10°$. Yet, the negative ones have the highest aerodynamic efficiency. By comparing $\Lambda = 20°$ case with the same angle of attack, $\Lambda = 30°$ resulted in less efficient L/D values over the same range of cant angles.

https://doi.org/10.55212/ijaa.1088399

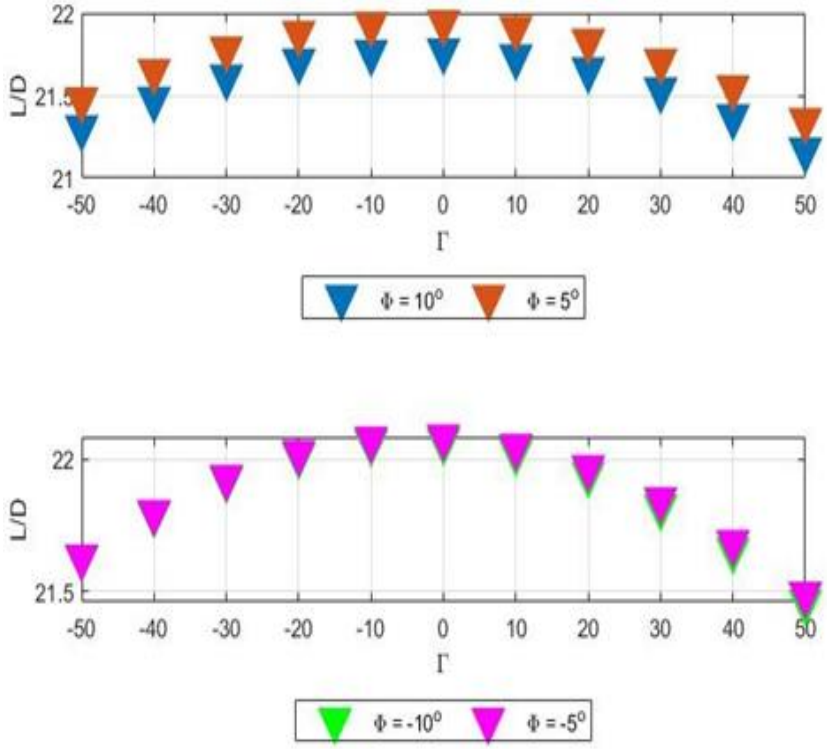

Fig. 12. Cant angle variation versus L/D at α = 4° and Λ = 30°

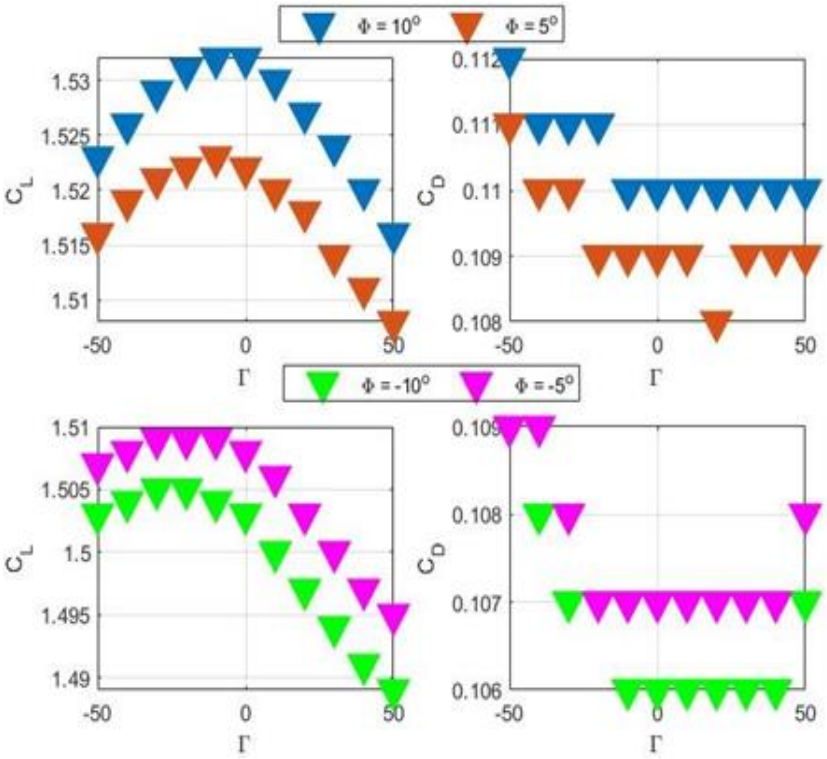

Fig. 13. Cant angle variation versus C_L and C_D at α = 12° and Λ = 30°. at α = 12◦ and Λ = 30◦

https://doi.org/10.55212/ijaa.1088399

Figure 13 represents the C_L and C_D variations over the same cant angle range at α = 12° and Λ = 30°. Unlike Λ = 20°, negative cant angles show improved C_L curves for positive twist values. Also, for negative twist cases, the negative cant angles give comparable results with each other. As the cant angle morphs from -50° to -10°, C_L tends to increase. After Γ = −10° has reached, all C_L curves have decreasing manner at α = 12° and Λ = 30°. Yet, α = 12°at Λ = 20° case has slightly higher C_L and C_D values. To compare L/D curves, Figure 14 shows the variation of analyzed twist values over the specified range of cant angles at α = 12° and Λ = 30°. It can be seen from the graph that the L/D values are increased with increasing the sweep angle. For positive twist angles, φ = 5° observed to have the highest aerodynamic efficiency with the cant angle of Γ = 10°.

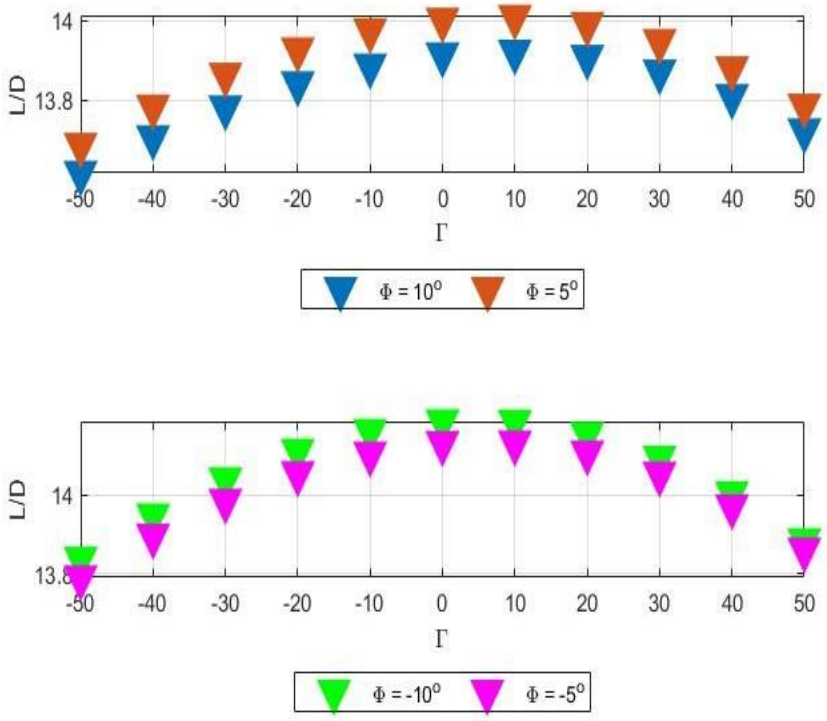

Fig. 14. Cant angle variation versus L/D at α = 12° and Λ = 30°

For negative twist values, Γ = 0° and Γ = 10° have the highest aerodynamic efficiency. By considering four twist angles, φ = -5° with Γ = 10° has the greatest aerodynamic efficiency at this flight regime. Unlike the case with Λ = 20°, the values for Γ = 0° increased. Comparing the case with Λ = 20° and the same angle of attack, Λ = 30° have higher aerodynamic efficiency over the same range of cant angles.

4. Conclusion

In this paper, variable winglet dihedral, twist, and wing-sweep concepts are numerically investigated. The computations consist of several configurations; for the variable-sweep concept, the values considered vary from Λ = 0 to Λ = 30◦, and for the winglet twist concept, φ = −10◦, −5◦, 5◦ and 10◦ cases were analyzed. The results show that variable-sweep angle increases the aerodynamic efficiency by morphing from unswept to swept-wing configurations. Moreover, variable winglet twist improves the performance of an aircraft in terms of drag reduction at different flight conditions and thus gives the optimum flight capabilities. By sweeping the wing, it is possible to obtain more than 9% increase in efficiency whereas the wing-tip twist concept provides a significant amount of drag reduction under certain conditions. Due to these benefits, it is important to assess and investigate the morphing phenomenon in order to bring it to practical use.

https://doi.org/10.55212/ijaa.1088399

References

[1] McRuer, D. and Graham, D. 2004. Flight Control Century: Triumphs of the Systems Approach, J. Guid. Control. Dyn., vol. 27, no. 2, pp. 161–173, doi: 10.2514/1.4586.

[2] McGowan, A., Vicroy, D., Busan, R. C. and Hahn, A. S. 2009. Perspectives on Highly Adaptive or Morphing Aircraft, RTO Appl. Veh. Technol. Panel Symp., pp. 1-1-1–14.

[3] Barbarino, S., Bilgen, O., Ajaj, R., M. Friswell, M. I. and Inman, D. J. 2011. A Review of Morphing Aircraft, J. Intell. Mater. Syst. Struct., vol. 22, no. 9, pp. 823–877, Aug., doi: 10.1177/1045389X11414084.

[4] Weisshaar, T. A. 2013. Morphing Aircraft Systems: Historical Perspectives and Future Challenges, J. Aircr., vol. 50, no. 2, pp. 337–353, doi: 10.2514/1.C031456.

[5] Jha, A. K. and Kudva, J. N. 2004. Morphing Aircraft Concepts, Classifications, and Challanges, Smart Structures and Materials, July, vol. 5388, San Diego, 213–224, doi: 10.1117/12.544212.

[6] Sofla, A. Y. N., Meguid, S. A., Tan, K. T. and Yeo, W. K. 2010. Shape morphing of aircraft wing: Status and challenges, Mater. Des., vol. 31, no. 3, March 1284–1292, doi: 10.1016/j.matdes.2009.09.011.

[7] Ajaj, R. M., Beaverstock, C. S. and Friswell, M. I. 2017. Morphing aircraft: The need for a new design philosophy, Aerosp. Sci. Technol., vol. 49, no. December, 154–166, 2015, doi: 10.1016/j.ast.2015.11.039.

[8] Thill, C., Etches, J., Bond, I., Potter, K., & Weaver, P. 2008. Morphing skins. The Aeronautical Journal (1968), 112(1129), 117-139. doi:10.1017/S0001924000002062

[9] Bubert, E. A. 2009. "Highly Extensible Skin for a Variable Wing-Span Morphing Aircraft Utilizing Pneumatic Artificial Muscle". Master thesis, The University of Maryland, College Park, Faculty of the Graduate School,Maryland, USA, 70-105.

[10] Perkins, D. A. 2005. Adaptive wing structures, Proc. SPIE, vol. 5762, pp. 132–142, [Online]. Available: http://link.aip.org/link/?PSI/5762/132/1&Agg=doi.

[11] Gandhi, F. and Anusonti-Inthra, P. 2008. Skin design studies for variable camber morphing airfoils, Smart Mater. Struct., vol. 17, no. 1, p. 015025, doi: 10.1088/0964-1726/17/01/015025.

[12] Hinshaw, T. 2009. "Analysis and Design of a Morphing Wing Tip using Multicellular Flexible Matrix Composite Adaptive Skins". Master thesis, Virginia Polytechnic Institute and State University, Virginia, USA, 20-85.

[13] Neal, & Anthony, D. 2006. "Design, Development, and Analysis of a Morphing Aircraft Model for Wind Tunnel Experimentation". Master thesis, Virginia Polytechnic Institute and State University, Virginia, USA, 17-107

[14] Blondeau, J., Richeson, J., Pines, D. J. and Norfolk, A. 2003. Design, development and testing of a morphing aspect ratio wing using an inflatable telescopic spar, 44th AIAA / ASME / ASCE / AHS Structures , Structural," Aerosp. Eng., vol. 1718, no. April, pp. 1–11.

[15] Joo. J. J. 2012. Optimal actuator location within a morphing wing scissor mechanism configuration, Proc. SPIE, vol. 6166, no. May, pp. 616603-616603–12, [Online]. Available: http://link.aip.org/link/PSISDG/v6166/i1/p616603/s1&Agg=doi.

[16] Dunbar, B. and Y. G., NASA Armstrong Fact Sheet: X-5 Research Aircraft, 2014. https://www.nasa.gov/centers/armstrong/news/FactSheets/FS-081-DFRC.html.(13 March 2022)

[17] Gatto, A., Mattioni, F. and Friswell, M. I. 2009. Experimental Investigation of Bistable Winglets to Enhance Aircraft Wing Lift Takeoff Capability, J. Aircr., vol. 46, no. 2, pp. 647–655, doi: 10.2514/1.39614.

[18] Kaygan, E. and Ulusoy, C. 2018. Effectiveness of Twist Morphing Wing on Aerodynamic Performance and Control of an Aircraft, J. Aviat., vol. 2, no. 2, 77–86, doi: 10.30518/jav.482507.

https://doi.org/10.55212/ijaa.1088399

[19] Cooper, J. E., Chekkal, I., Cheung, R. C. M., Wales, C., Allen, N. J., Lawson, S., Peace, A. J., Cook, R., Standen, P., Hancock S. D. and Carossa, G. M. 2015. Design of a morphing wingtip, J. Aircr., vol. 52, no. 5, pp. 1394–140, doi: 10.2514/1.C032861.

[20] Kaygan, E. 2020. Aerodynamic Analysis of Morphing Winglets for Improved Commercial Aircraft Performance, J Aviat, vol. 4, no. 1, pp. 31–44, [Online]. Available: https://doi.org/10.30518/jav.716194.

[21] Bourdin, P., Gatto, A. and Friswell, M. I. 2010. Performing co-ordinated turns with articulated wing-tips as multi-axis control effectors, Aeronaut. J., vol. 114, no. 1151, pp. 35–47.

[22] Kaygan, E. and Gatto, A. 2014. Investigation of Adaptable Winglets for Improved UAV Control and Performance. Int. J. Aerosp. Mech. Eng.,vol. 8, no. 7, pp. 1281–1286.

[23] Kaygan, E. and Gatto, A. 2016. Development of an Active Morphing Wing With Adaptive Skin for Enhanced Aircraft Control and Performance. Greener Aviation 2016, October.

[24] Kaygan, E. and Gatto, A. 2018. Structural Analysis of an Active Morphing Wing for Enhancing Unmanned Aerial Vehicle Performance. Int. J. Aerosp. Mech. Eng., vol. 12, no. 10, pp. 948–955.

[25] Gatto, A., Bourdin, P. and Friswell, M. I. 2010. Experimental Investigation into Articulated Winglet Effects on Flying Wing Surface Pressure Aerodynamics, J. Aircr., vol. 47, no. 5, pp. 1811–1815, doi: 10.2514/1.C000251.

[26] Woods, B. K., Bilgen, O. and Friswell, M. I. 2014. Wind tunnel testing of the fish bone active camber morphing concept, J. Intell. Mater. Syst. Struct., vol. 25, no. 7, pp. 772–785, Feb., doi: 10.1177/1045389X14521700.

[27] Hepperle, M. 2011. JAVAFOIL user's guide, 2011. https://www.mh-aerotools.de/airfoils/java/JavaFoil Users Guide.pdf. (23 July 2021.)

[28] Drela, M. 1989. XFOIL: An Analysis and Design System for Low Reynolds Number Airfoils. Lecture Notes in Engineering, vol 54. Springer, Berlin, Heidelberg. https://doi.org/10.1007/978-3-642-84010-4_1

[29] Saffman, P. G. Vortex Dynamics, Cambridge Univ. Press, United Kingdom, 1992.

[30] Anderson, J. D. Fundamentals of Aerodynamics, Sixth. McGraw- Hill Education, USA, 2017.

[31] Gudmundsson, S. 2014. The Anatomy of the Wing. General Aviation Aircraft Design, pp. 299-399, doi: 10.1016/B978-0-12-397308-5.00009-X.

[32] Page, R. K. 1968. Aircraft with Variable-Sweep Wings. Aircr. Eng. Aerosp. Technol., vol. 37, no. 10, pp. 295–299, doi: 10.1108/eb034081.

[33] Mulyanto, T., Lutfhi, M., Nurhakim, I. and Sasongko, R. A. 2010. Development of A Morphing Flying Platform for Adaptive Cotrol System Study. ICAS2010, pp. 1–5.

[34] Kaygan, E. and Gatto, A. 2014. Investigation of Adaptable Winglets for Improved UAV Control and Performance. Int. J. Mech. Aerospace, Ind. Mechatronics Eng., vol. 8, no. 7, pp. 1281–1286.

[35] Phillips, W. F., Alley, N. R. and Goodrich, W. D. 2004. Lifting-Line Analysis of Roll Control and Variable Twist. J. Aircr., vol. 41, no. 5, pp. 1169–1176, doi: 10.2514/1.3846.

[36] Guerrero, J. E., Sanguineti, M. and Wittkowski, K. 2020. Variable cant angle winglets for improvement of aircraft flight performance. Meccanica, vol. 55, no. 10, pp. 1917–1947, doi: 10.1007/s11012-020-01230-1.

[37] Bourdin, P., Gatto, A. and Friswell, M. I. 2008. Aircraft Control via Variable Cant-Angle Winglets. Journal of Aircraft, vol. 45, no. 2. pp. 414–423.

[38] Gatto, A., Bourdin, P. and Friswell, M. I. 2012. Experimental investigation into the control and load alleviation capabilities of articulated winglets. Int. J. Aerosp. Eng., vol. 1, doi: 10.1155/2012/789501.

https://doi.org/10.55212/ijaa.1088399